# On the elastodynamic properties of octet truss-based architected metamaterials

Mourad Oudich, Edward Huang, Hyeonu Heo, Zhenpeng Xu, Huachen Cui, Nikhil Jrk Gerard, Xiaoyu Rayne Zheng, Yun Jing

# On the elastodynamic properties of octet truss-based architected metamaterials

Mourad Oudich,[1,2,†] Edward Huang,[3] Hyeonu Heo,[1] Zhenpeng Xu[4], Huachen Cui[4], Nikhil JRK Gerard[1], Xiaoyu (Rayne) Zheng[4,5,*], and Yun Jing[1,‡]

[1]*Graduate Program in Acoustics, The Pennsylvania State University, University Park, PA 16802*

[2]*Université de Lorraine, CNRS, Institut Jean Lamour, F-54000 Nancy, France*

[3]*William G. Enloe Magnet High School, Raleigh, NC 27610*

[4]*Department of Civil and Environmental Engineering, University of California, Los Angeles, California 90095, USA*

[5]*Department of Materials Science and Engineering, University of California, Berkeley, California, 94720, USA*

†mxo5236@psu.edu

*rayne23@berkeley.edu

‡yqj5201@psu.edu

**ABSTRACT**

Architected metamaterials have emerged as a central topic in materials science and mechanics thanks to the rapid development of additive manufacturing techniques, which has enabled new families of artificial materials with outstanding mechanical properties. This letter seeks to investigate the elastodynamic behavior of octet truss lattices as an important type of architected metamaterials for high effective strength and vibration shielding. We design, fabricate, and experimentally characterize three types of octet truss structures, including two homogenous structures with either thin or thick struts and one hybrid structure with alternating strut thickness. High elastic wave transmission rate is observed for the lattice with thick struts, while strong vibration mitigation is captured from the homogenous octet truss structure with thin struts as well as the hybrid octet truss lattice, though the underlying mechanisms for attenuation are fundamentally different (viscoelasticity induced dampening vs. band gaps). Compressional tests are also conducted to evaluate the effective stiffness of the three lattices. This study could open a new avenue toward multifunctional architected metamaterials for vibration shielding with high mechanical strength.

**Keywords**; Architected metamaterials, octet truss, elastodynamic properties

## INTRODUCTION

Architected metamaterials are engineered structures and/or material compositions that can provide unprecedented mechanical and dynamic properties – low density coupled with high strength and stiffness[1,2], negative Poisson's ratio[3], negative stiffness for energy absorption[4,5], negative thermal expansion coefficient[6], and vibration control[7–16]. They are generally built with connected struts and masses in a sophisticated design configuration to achieve the abovementioned behaviors and functionalities. In particular, octet truss based architected metamaterial (OTAM)[17] is a structure best known for its high strength-to-weight ratio due to its stretch-dominated architecture[18]. The highly connected node networks in the OTAM structure provide outstanding stiffness with low density[1]. In addition, the deformation mechanism of OTAMs endows them with excellent energy absorption capability[19–21], therefore making them promising candidates for lightweight protection materials[22]. While OTAM have been primarily studied for their mechanical (quasi-static) properties, their elastodynamic behaviors remain elusive in the context of stress wave propagation. Messener et al.[23] theoretically characterized the effective dynamic properties of a periodic octet truss structure by evaluating the elastic wave dispersion relation at the long-wavelength regime. Beyond this approximative dynamic description of the lattice based on homogenization theory, further investigation of the elastodynamic properties of OTAMs is important as they could be proven a useful multifunctional material for providing outstanding load resistance and vibration attenuation. This constitutes the motivation for this study.

Targeting multifunctional capability, several studies delt with engineering lightweight architected metamaterials for sound and vibration control with high mechanical strength. These investigations included static mechanical behavior with blast protection capability[24,25], high stiffness panels for sound absorption[26,27], and vibration attenuation with controllable Poisson ratio[28] and mechanical strength[29,30]. The present work, however, focuses specifically on the octet truss lattice that presents good mechanical strength but has limited vibration attenuation ability. Our purpose is to address this performance limitation for vibration mitigation by considering a hybrid design of the octet truss building.

There are two main mechanisms that could be at play for vibration attenuation: energy dissipation (e.g., due to the viscoelasticity of the intrinsic material) and reflection (due to the presence of bandgaps (BGs)). In engineering applications, energy dissipation is the primary means for vibration attenuation (e.g., rubber vibration isolators). However, BG-based vibration reduction can potentially lead to a greater amount of transmission loss. Very recently, Aguzzi et al.[31,32] investigated the wave dispersion for a plate made of octet truss lattice and showed BGs at low frequency. Although their plate-type octet truss structure shows promising performance for vibration mitigation, it was designed for controlling plate waves. In this present work, we consider the octet truss lattice as a truly 3D lattice (rather than a 2D plate structure) for bulk

vibration mitigation which is fundamentally different from that of Aguzzi et al.[31,32] . The bulk wave velocity is in general greater than that of plate waves when the plate thickness is comparable to wavelength. Consequently, the wave dispersion by a periodic lattice is produced at higher frequencies for bulk waves in comparison with the case of a plate structure. Our 3D OTAM lattices are designed for bulk wave dispersion and attenuation, where the challenge is to achieve these functionalities at low frequencies. Further, we also consider hybrid OTAMs for the purpose of low frequency vibration shielding with BGs that otherwise would not exist at the specific period under study with the permissible strut size.

In this letter, we study the OTAMs where particular attention is brought to the structural design and the lattice's elastodyanmic properties to achieve vibration attenuation while maintaining its excellent mechanical property. Three designs of OTAM are considered: OTAM with thin struts, thick struts, and hybrid OTAM made by alternating octet truss units with thin and thick struts. For each OTAM design, the elastodynamic properties have been investigated using numerical analysis and experimental realization via a 3D printing technique followed by dynamic and static characterizations to evaluate its capability to attenuate vibration and its mechanical strength.

The three OTAMs are periodic lattices of octet truss units made of cylindrical struts (rods) having the same diameter (**Fig. 1(a)**). The unit cell length (period) is $a = 1.5$ cm. Throughout this study, the material mechanical properties used in the numerical simulation are those of the polymeric material used in 3D printing, which are: the density $\rho = 1{,}175.5\ kg/m^3$, the Young's modulus $E = 3$ GPa, and the Poisson's ratio $\nu = 0.46$. To determine these properties, samples of the polymeric material were printed and tested on MTS Criterion – model 43 with 20 kN loadcell and video extensometer, MTS Systems. The specimen size follows ASTM E8 standard tensile test method. At room temperature (22°C), the tensile force on the specimen was measured with a load cell under 0.01mm/s overhead displacement. Simultaneously, longitudinal and transverse strains were recorded by the video extensometer and used to determine Young's modulus and Poisson's ratio of the printed materials. Furthermore, as the used polymeric material is viscoelastic, we performed multifrequency dynamic tests to measure the dynamic modulus and the mechanical loss factor via Q800 dynamic mechanical analysis (DMA), TA instruments. In a dynamic tension mode, an oscillating force was applied to the sample, and the sample's response to the force was analyzed via the time-temperature superposition analysis.[33] Consequently, we considered the approximate value of 0.12 for the loss factor in the numerical simulations for evaluating the wave transmission through the OTAMs and the hybrid OTAM.

We first calculated the dispersion curves for the three OTAM lattices by considering a unit cell (**Fig. 1**) using the eigenfrequency analysis in the commercial software COMSOL Multiphysics. The first OTAM was made of rods with a diameter of 3 mm (**Fig. 1(a)** bottom left panel), the second one was with 1 mm

diameter (**Fig. 1(a)** bottom right panel), and the third OTAM was made by alternating octet truss units with rod diameters 1 mm and 3 mm (**Fig. 1(b)**). We refer to this third lattice as the hybrid OTAM (HOTAM). The two OTAMs are periodic in all three directions in space, so an octet truss unit cell was considered with periodic boundary conditions in all three directions for the band structure calculation. For the HOTAM, since the periodic alternation of the octet truss units with different diameters is along the *x* direction in space (**Fig. 1(b)**), the periodicity is 3 cm along this direction, while it is 1.5 cm along *y* and *z* directions. We limit our dispersion calculation to the Γ-Z direction in the irreducible Brillouin zone, which corresponds to the propagation direction along the octet truss units' alternation in the HOTAM, and because the wave transmission will be studied only in this same direction later in the study. We note that this direction is consistent with the loading direction of octet truss lattices. The full band structure of the HOTAM lattice is presented in the Supplementary Material.

In the case of thick rods OTAM (3 mm diameter), the band structure shows no dispersion up to 20 kHz, while for frequencies higher than 20 kHz the lattice displays strong band dispersion but with no BGs (**Fig. 1(a)** bottom left panel). However, when considering the OTAM with thin rods (1 mm diameter), strong band dispersion is depicted starting from 7.87 kHz with no BG as well (**Fig. 1(a)** bottom left panel). For the case of HOTAM, several BGs can be seen below 15 kHz with the lowest one extending from 5.4 kHz to 8.6 kHz (**Fig. 1(b)**). The alternation of the rods diameter from one octet truss unit to the adjacent one induces a periodic change in the effective stiffness of the HOTAM as the octet truss units with thick rods display a higher effective stiffness than that of the units with thin rods. This makes the HOTAM a phononic crystal with BGs. These BGs are created by by the mechanism of Bragg scattering caused by the periodicity of the lattice[34].

We then fabricated samples to study the dynamic and quasi-static behaviors of the three lattices. We chose to make samples of 5x2x2 octet truss units (insets in **Fig.2 (b)-(d)**). The fabrication of the OTAM and HOTAM samples was made possible by stereolithography (SLA) using a Formlab Form 3+ 3D printer. All microstructures were fabricated with a specific orientation, approximately 30° tilted from the normal to the horizontal plane, to avoid internal support structures within the lattices from the 3D printing. The selected printing resolution had a layer thickness of 25 μm.. While the two OTAMs were made with struts of 1 and 3 mm diameters, the HOTAM was constructed by alternating rods diameter of the units starting with 3 mm at the base (see inset in **Fig. 2(d)**). In addition to the lattice-based microstructure, the fabricated samples have plates with a thickness of 3mm on both ends for the convenience of the experimental characterization. The samples were tested immediately after fabrication to preserve the initial constituent material stiffness as the material gets hardened over time, particularly when

exposed to light. Three samples were fabricated for each design, which allowed us to evaluate the standard derivation of experimental results.

The elastic wave transmission measurements through the OTAM and HOTAM samples were carried out by connecting a K2004E01-SU Mini Shaker into the plate on one end of the sample, and the shaker was connected to a function (signal) generator, PicoScope (series 5000), that facilitates the longitudinal wave excitations. The plate of the other end of the sample was connected to an accelerometer (PCB Piezotronics 352C67 (100mV/g)) to measure the transmitted wave through the sample from one end to the other. The accelerometer was connected to a PCB Piezotronics ICP Sensor Signal Conditioner (482B11), which amplifies the acquired signal and transmits the data into a PicoScope (series 5000 oscilloscopes). The reference frequency of the PicoScope was programmed to drive the mechanical shaker to cycle from 2 kHz to 15 kHz, at an amplitude of 60 mV, with an incrementation of 100 Hz every second (**Fig. 2(a)**).

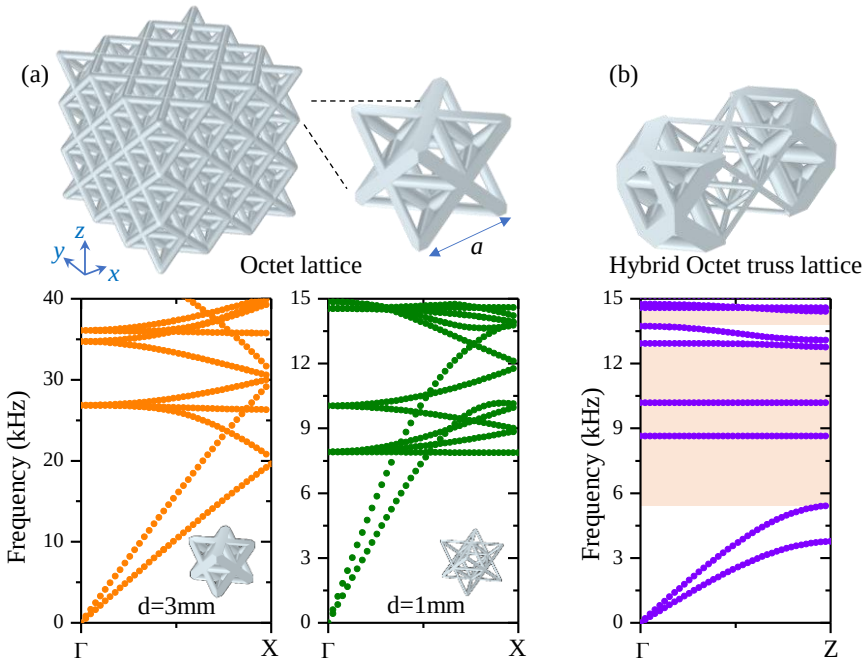


**Fig. 1.** (a) Octet truss lattice with unit cell (Upper panel). Band structures for the case of struts diameter of 3mm and 1mm (bottom panel). (b) Hybrid octet truss lattice made of alternating octet truss unit cells with different struts diameters (1mm and 3mm). The band structure shows the appearance of BGs (Bottom panel, shaded regions). Note the different frequency ranges in the band structures.

The measured transmission curves for the OTAMs and HOTAM samples are presented in **Figs. 2(b)-(d),** along with the numerically calculated transmission (via COMSOL) for the sake of comparison. In the case of OTAM with thick rods (3 mm diameter), relatively strong wave transmission is depicted in both measurement and simulation in the range of frequencies 2 to 15 kHz, except for the presence of a dip at

14.2 kHz, which is likely due to the anti-resonance of the plate in contact with the shaker (**Fig. 2(b)**). This dip is also depicted but at a higher frequency (a little above 15 kHz) in the measurement. However, in the case of OTAM with thin rods (1 mm), the experimental and calculated transmissions show a significant drop from 6 kHz to higher frequencies (**Fig. 2(c)**), though the dispersion curve calculation does not show any presence of BGs (**Fig. 1(a)**). This drop is caused by the viscoelastic loss of the used polymeric materials as thin rods support high order modes at this range of frequency that can be damped by the loss. Good agreement is found between simulation and measurement results. In the case of HOTAM, strong wave attenuation is observed between 6 and 12 kHz with relatively good agreement between the measured and calculated transmissions (**Fig. 2(d)**). This wave attenuation is caused by the presence of the BG from the periodicity of the hybrid lattice. A discussion about the effect of viscoelasticity in HOTAM is presented in the Supplementary Maerial. In summary, accessing wave attenuation with octet truss lattices below 15 kHz with the period of 1.5 cm can be achieved via the HOTAM using the BG or the OTAM with thin rods via viscoelasticity of the polymeric material. However, it is expected that the two samples would show different mechanical strengths.

In order to measure the effective mechanical properties of the three architected metamaterials, compressional tests were performed using QTest 100 (100kN frame) with 10 kN loadcell, MTS Systems (**Fig. 3(a)**). The experiment was conducted with 0.01mm/s overhead displacement while the reaction force was measured through the load cell at room temperature (22°C). Based on measured stress and strain, the effective stiffness and ultimate strength of each specimen were determined. **Figures 3(b)-(d)** show the strain/stress curves for the OTAMs with rods thickness of 3 mm (**Fig. 3(b)**) and 1 mm (**Fig. 3(c)**), and for the HOTAM (**Fig. 3(d)**). From these curves, we deduced the effective stiffness and the ultimate strength for the three structures which are summarized in **Table 1**. The 3D printed OTAM lattices were made of a strong polymer (Formlabs, clear resin) which has a stiffness of 3 GPa and good toughness. In the compression test, we observed that the stress of OTAM with thin rods reaches its peak value when the lattice reaches its elastic limit, after which stage the stress drops due to the buckling of the struts. For OTAM with thick rods, the lattice shows a typical ductile behavior, with fracture occurring at a high level of strain. No buckling was observed due to the low aspect ratio of the struts. For the HOTAM, we observed local buckling at the layer with thinner rods after the linear region. With further increase in strain, local fractures were observed at the junction of thin and thick rods (See videos of the tests in the Supplementary Material). Furthermore, the high brittle response of HOTAM compared with OTAM with thick rods is mainly due to thin strut thickness and local rupture. For HOTAM, the buckling stress of the lattice depends on thin struts rather than thick struts if considering a compression direction of (1,0,0), as presented in this work. Therefore, the HOTAM shows lower stiffness than the OTAM with thick rods. We observed some local fractures

during the compression test of HOTAM, which can be attributed to stress concentrations at the junction of thin and thick rods.

From **Table 1**, It is clear that the effective stiffness and strength of the OTAM with thick rods (3mm diameter) are one order of magnitude higher than those of the OTAM with thin rods (1mm) and the HOTAM. Nevertheless, although the stiffness of the HOTAM is one order of magnitude higher than that of the OTAM with 1 mm rod diameter, the density of the HOTAM is 4.6 times larger which leads to a slightly lower normalized stiffness of the HOTAM in comparison to the OTAM. Besides, the ultimate strength of HOTAM remains higher than that of the OTAM. In short, though the OTAM with thick rods displays high mechanical strength, its ability to shield elastic waves is limited in comparison to the OTAM with thin rods, which has the drawback of having poor mechanical strength. A combination between the two OTAMs which gives the HOTAM increases the ultimate strength while providing the ability to shield vibration using the mechanism of BG.

In conclusion, we have investigated the mechanical strength and elastodynamic properties of three types of octet truss lattices: two OTAMs with homogenous struts diameters and a hybrid OTAM with alternating octet truss units with different rod diameters. The OTAM with thick rods (3 mm) displays high effective stiffness and ultimate strength but has a low capability for attenuating vibration at low frequencies (below 13 kHz). However, although the rod's diameter can be lowered to enable the OTAM capability for elastic wave shielding via the viscoelastic effect, its stiffness and strength are lowered by almost two orders of magnitude, which may hinder its usability. Combining the two OTAM designs by alternating the octet truss units with different rod diameters, on the other hand, increases the effective stiffness of the lattice while endowing the structure with the ability of elastic wave mitigation through the mechanism of BG. The present study could open routes towards heterogeneous design of 3D architected lattices with increased mechanical strength while providing opportunities for vibration control.

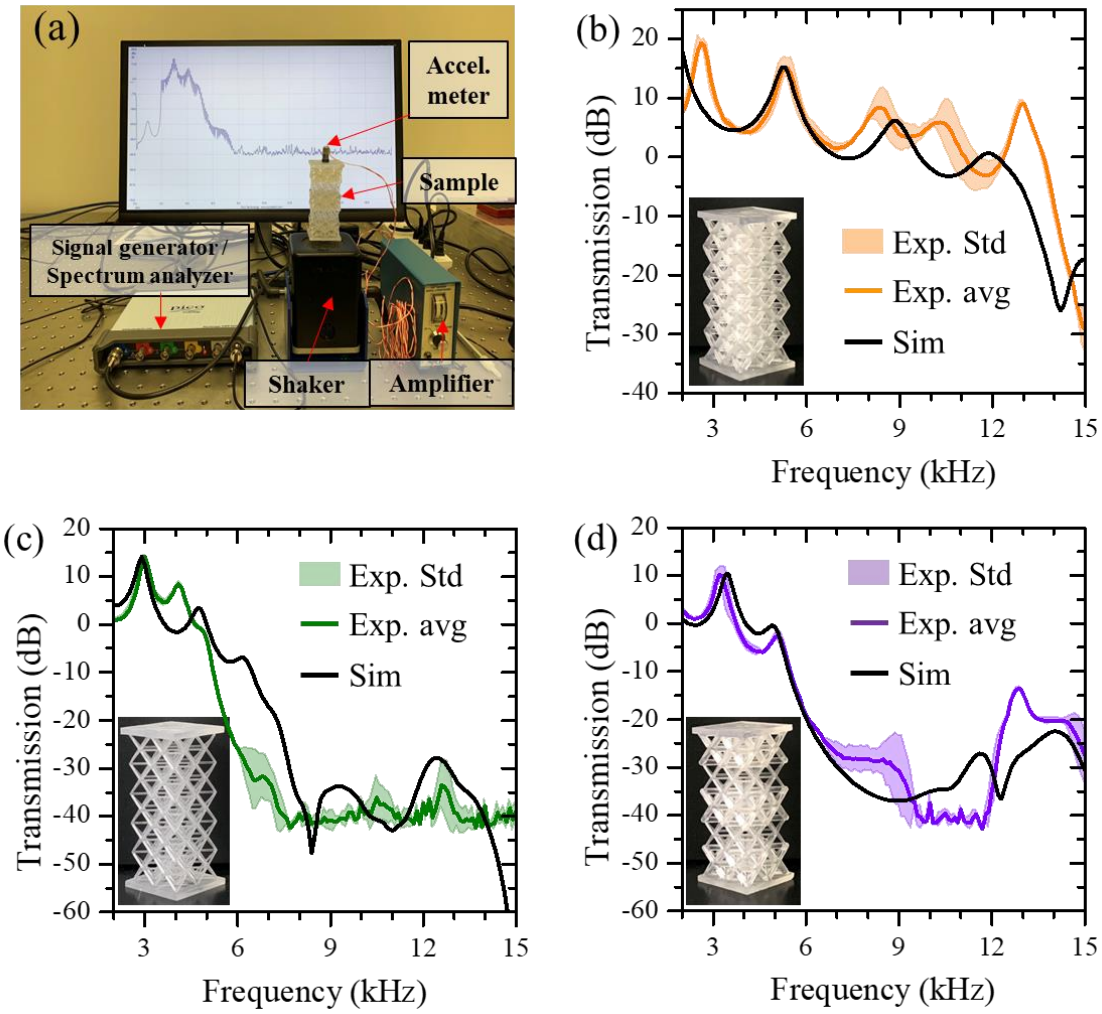


**Fig. 2**. (a) Experimental setup for measuring the elastic wave transmission through the OTAM and HOTAM samples. A shaker is used for wave excitation, and an accelerometer is used for measuring the transmitted wave. (b)-(c) Experimental measurements (colored solid lines) and numerical calculations (solid black lines) of the wave transmission as a function of the frequency for OTAMs with rods thicknesses 3mm (orange line in (b)) and 1mm (green line in (c)), and the HOTAM (purple line in (d)). The shaded region on the colored curves marks the error areas deduced from standard deviation of the repeated measurements.

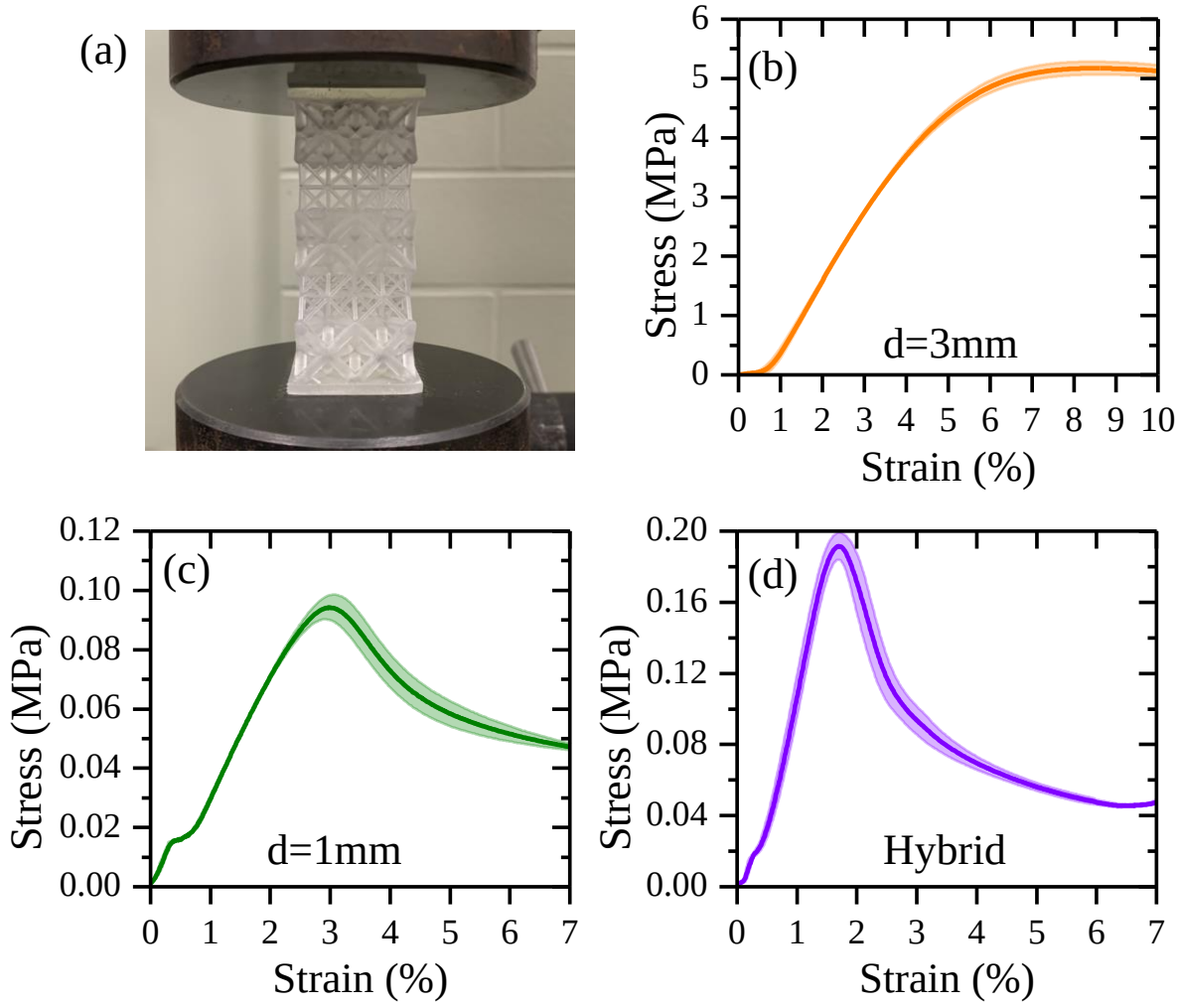


**Fig. 3**. (a) Compressional test on the OTAM and HOTAM. (b)-(d) Compression test results as the measured stress-strain curve for the OTAMs with rods diameter 3mm (b) and 1mm (c), as well as for the HOTAM (d).

| | OTAM with 3mm | OTAM with 1mm | HOTAM |
|---|---|---|---|
| Effective density $\rho_{eff}$ (kg/m$^3$) | 444.67 | 62.82 | 291.51 |
| Relative density $(\bar{\rho} = \rho_{eff}/\rho_0)$ | 37.83% | 5.34 % | 24.80% |
| Effective stiffness $E_{eff}$ (MPa) | 121.98 | 4.20 | 16.71 |
| Normalized stiffness $E_{eff}/\bar{\rho}$ (MPa) | 322.46 | 78.60 | 67.38 |
| Ultimate strength (MPa) | 5.33 | 0.11 | 0.20 |

**Table 1**. Effective mechanical properties of the OTAMs and HOTAM samples.

## ACKNOWLEDGEMENTS

We would like to thank Garret Corso at the Materials Research Institute, Penn State University, for performing the material's tensile tests and DMA. We also thank Dr. Henrietta Tsosie at the Department of Engineering Science and Mechanics, Penn State University, for assisting with the compression test. YJ thanks the NSF DMREF for the support through CMMI 2119545. XZ thanks the NSF DMREF for the support through CMMI 2119643 and AFOSR (FA9550-18-1-0299).

## DATA AVAILABILITY

The data that support the findings of this study are available from the corresponding author upon reasonable request.

## REFERENCES

[1] X. Zheng, H. Lee, T.H. Weisgraber, M. Shusteff, J. DeOtte, E.B. Duoss, J.D. Kuntz, M.M. Biener, Q. Ge, J.A. Jackson, S.O. Kucheyev, N.X. Fang, and C.M. Spadaccini, Science **344**, 1373 (2014).
[2] X. Zheng, W. Smith, J. Jackson, B. Moran, H. Cui, D. Chen, J. Ye, N. Fang, N. Rodriguez, T. Weisgraber, and C.M. Spadaccini, Nat. Mater. **15**, 1100 (2016).
[3] D. Chen and X. Zheng, Sci. Rep. **8**, 9139 (2018).
[4] C.S. Ha, R.S. Lakes, and M.E. Plesha, Int. J. Solids Struct. **178–179**, 127 (2019).
[5] C.S. Ha, R.S. Lakes, and M.E. Plesha, Mater. Des. **141**, 426 (2018).
[6] H. Heo, S. Li, H. Bao, and J. Ju, Adv. Eng. Mater. **21**, 1900225 (2019).
[7] S. Taniker and C. Yilmaz, Int. J. Solids Struct. **72**, 88 (2015).
[8] K.H. Matlack, A. Bauhofer, S. Krödel, A. Palermo, and C. Daraio, Proc. Natl. Acad. Sci. **113**, 8386 (2016).
[9] L. D'Alessandro, E. Belloni, R. Ardito, F. Braghin, and A. Corigliano, Appl. Phys. Lett. **111**, 231902 (2017).
[10] F. Warmuth, M. Wormser, and C. Körner, Sci. Rep. **7**, 3843 (2017).
[11] L. D'Alessandro, V. Zega, R. Ardito, and A. Corigliano, Sci. Rep. **8**, 2262 (2018).
[12] W. Elmadih, D. Chronopoulos, W.P. Syam, I. Maskery, H. Meng, and R.K. Leach, Sci. Rep. **9**, 11503 (2019).
[13] X. Fei, L. Jin, X. Zhang, X. Li, and M. Lu, Appl. Phys. Lett. **116**, 021902 (2020).
[14] N.J. Gerard, M. Oudich, Z. Xu, D. Yao, H. Cui, C.J. Naify, A. Ikei, C.A. Rohde, X. (Rayne) Zheng, and Y. Jing, Phys. Rev. Appl. **16**, 024015 (2021).
[15] Muhammad and C.W. Lim, Sci. Rep. **11**, 7137 (2021).
[16] Z. Xu, R. Hensleigh, N.J. Gerard, H. Cui, M. Oudich, W. Chen, Y. Jing, and X. (Rayne) Zheng, Addit. Manuf. **47**, 102321 (2021).
[17] V.S. Deshpande, N.A. Fleck, and M.F. Ashby, J. Mech. Phys. Solids **49**, (2001).
[18] L. Dong, V. Deshpande, and H. Wadley, Int. J. Solids Struct. **60–61**, 107 (2015).
[19] T. Tancogne-Dejean, A.B. Spierings, and D. Mohr, Acta Mater. **116**, 14 (2016).
[20] M. Mieszala, M. Hasegawa, G. Guillonneau, J. Bauer, R. Raghavan, C. Frantz, O. Kraft, S. Mischler, J. Michler, and L. Philippe, Small **13**, 1602514 (2017).

[21] Z. Xu, C.S. Ha, R. Kadam, J. Lindahl, S. Kim, H.F. Wu, V. Kunc, and X. Zheng, Addit. Manuf. **32**, 101106 (2020).
[22] S. Mora, N.M. Pugno, and D. Misseroni, Mater. Today (2022).
[23] M.C. Messner, M.I. Barham, M. Kumar, and N.R. Barton, Int. J. Solids Struct. **73–74**, 55 (2015).
[24] A.G. Evans, J.W. Hutchinson, and M.F. Ashby, Prog. Mater. Sci. **43**, 171 (1998).
[25] H.N.G. Wadley, Philos. Trans. R. Soc. Math. Phys. Eng. Sci. **364**, 31 (2005).
[26] B. Han, Z.-J. Zhang, Q.-C. Zhang, Q. Zhang, T.J. Lu, and B.-H. Lu, Extreme Mech. Lett. **10**, 58 (2017).
[27] Y. Tang, S. Ren, H. Meng, F. Xin, L. Huang, T. Chen, C. Zhang, and T.J. Lu, Sci. Rep. **7**, 43340 (2017).
[28] Y. Chen, T. Li, F. Scarpa, and L. Wang, Phys. Rev. Appl. **7**, 024012 (2017).
[29] A.S. Phani, J. Woodhouse, and N.A. Fleck, J. Acoust. Soc. Am. **119**, 1995 (2006).
[30] I. Arretche and K.H. Matlack, Front. Mater. **5**, (2018).
[31] G. Aguzzi, C. Kanellopoulos, R. Wiltshaw, R.V. Craster, E.N. Chatzi, and A. Colombi, Sci. Rep. **12**, 1088 (2022).
[32] G. Aguzzi, H.R. Thomsen, A. Hejazi Nooghabi, R. Wiltshaw, R.V. Craster, E.N. Chatzi, and A. Colombi, Appl. Phys. Lett. **121**, 201702 (2022).
[33] C. Pasini, N. Inverardi, D. Battini, G. Scalet, S. Marconi, F. Auricchio, and S. Pandini, Smart Mater. Struct. **31**, 095021 (2022).
[34] M. Oudich, N.J. Gerard, Y. Deng, and Y. Jing, Adv. Funct. Mater. 2206309 (2022).